Applied Physics Letters

Nitrogen plasma passivated niobium resonators for superconducting quantum circuits

Cite as: Appl. Phys. Lett. **120**, 102601 (2022); https://doi.org/10.1063/5.0082755
Submitted: 17 December 2021 • Accepted: 24 February 2022 • Published Online: 11 March 2022

K. Zheng, D. Kowsari, N. J. Thobaben, et al.

Applied Physics Letters ARTICLE scitation.org/journal/apl

Nitrogen plasma passivated niobium resonators for superconducting quantum circuits

Cite as: Appl. Phys. Lett. **120**, 102601 (2022); doi: 10.1063/5.0082755
Submitted: 17 December 2021 · Accepted: 24 February 2022 ·
Published Online: 11 March 2022

View Online Export Citation CrossMark

K. Zheng,[1] D. Kowsari,[1] N. J. Thobaben,[2] X. Du,[1] X. Song,[1] S. Ran,[1] E. A. Henriksen,[1,3] D. S. Wisbey,[2] and K. W. Murch[1,a)]

AFFILIATIONS

[1]Department of Physics, Washington University, St. Louis, Missouri 63130, USA
[2]Department of Physics, Saint Louis University, St. Louis, Missouri 63103, USA
[3]Institute of Materials Science and Engineering, Washington University, St. Louis, Missouri 63130, USA

[a)]Author to whom correspondence should be addressed: murch@physics.wustl.edu

ABSTRACT

Microwave loss in niobium metallic structures used for superconducting quantum circuits is limited by a native surface oxide layer formed over a timescale of minutes when exposed to an ambient environment. In this work, we show that nitrogen plasma treatment forms a niobium nitride layer at the metal–air interface, which prevents such oxidation. X-ray photoelectron spectroscopy confirms the doping of nitrogen more than 5 nm into the surface and a suppressed oxygen presence. This passivation remains stable after aging for 15 days in an ambient environment. Cryogenic microwave characterization shows an average filling-factor-adjusted two-level-system loss tangent $F\delta_{TLS}$ of $(2.9 \pm 0.5) \cdot 10^{-7}$ for resonators with a 3 μm center strip and $(1.0 \pm 0.3) \cdot 10^{-7}$ for a 20 μm center strip, exceeding the performance of unpassivated samples by a factor of four.

Increasing the coherence time of superconducting qubits while maintaining reasonable gate speeds enables more powerful quantum processors.[1,2] The improvement in fabrication techniques plays an important role in this effort.[3,4] The fabrication process of high coherence planar superconducting quantum processors now typically involves two superconducting layers. The first layer makes up the ground plane and all the circuit elements other than the Josephson junction[5,6] (JJ) while the second layer defines the JJs. The two-layer process allows optimization of the quality factor of the superconducting capacitor pads independent from the requirements of the double-angle-evaporated aluminum JJ layer. Microwave coplanar waveguide (CPW) resonators have been demonstrated as a robust platform to characterize the microwave loss in superconducting materials[7,8] and have been instrumental in the continuous improvement of film and device quality.[9,10] In typical device geometries, less than 1 percent of the electric field energy is stored in the thin dielectric layers at the metal–air (MA), metal–substrate (MS), and substrate-air (SA) interfaces.[11,12] These dielectric layers may host two-level-system (TLS)[13] defects resulting in a high loss tangent[7,11,12] that dominates the single-photon energy loss of state-of-the-art superconducting devices, despite the small participation of these dielectric layers. For Nb resonators, the primary TLS loss comes from the oxide layer[14,15] at the MA interface. As the electric field energy stored in a thin dielectric layer at the interface is proportional to its thickness,[16] the removal of the oxide results in lower microwave loss. The removal of the surface oxide layer in Nb CPW resonators has resulted in single-photon internal quality factors Q_i up to 5×10^6 (Ref. 17) and filling factor adjusted two-level-system loss tangents $F\delta_{TLS}$ down to $9 \cdot 10^{-8}$. However, the oxide grows back following a Cabrera–Mott[18] behavior within several hours, reintroducing TLSs at the MA interface[16,19] (Fig. 1). As the buffered oxide etch (BOE) used to etch NbO_x also etches the Al JJ,[20] it is difficult to incorporate Nb resonators with a low density of TLSs at the MA interface into superconducting quantum circuits.

Nitride superconductors, such as NbN and TiN, are known to only have a thin native surface oxide layer at room temperature and, therefore, are expected to have fewer TLSs at the MA interface.[21] As for the MS interface, recent studies[22–25] have shown that high-quality TiN (200) films can be deposited directly on the Si substrate without a SiN_x seed layer deposited in a separate process step, which reduces the total microwave loss. However, the microwave loss of TiN at the MS interface is still higher than elemental superconductors, and work is needed to further improve the quality of the MS interface.[12] Resonators with Q_i on the order of 1×10^6 have been fabricated using sputtered and atomic-layer-deposited NbN thin films,[26,27] and

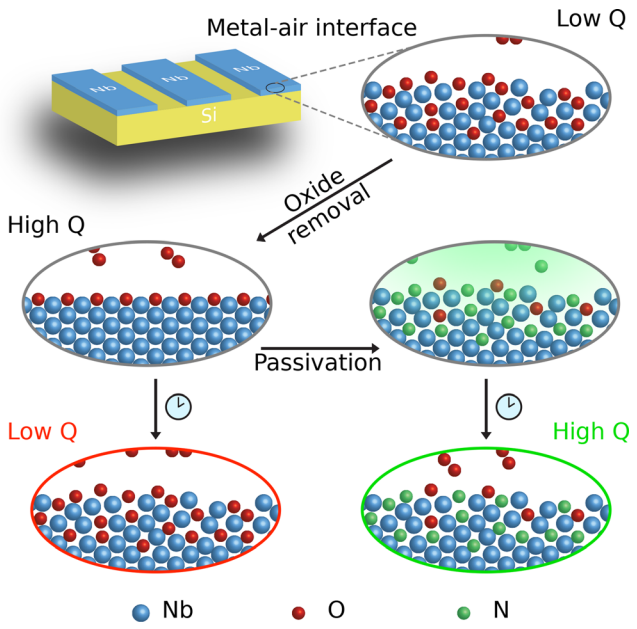

FIG. 1. Nitrogen passivation of Nb resonators. Nb films grow an amorphous oxide layer at the MA interface that results in a low quality factor. Removal of this oxide with a BOE clean improves Q, but the oxide regrows over time (left). Passivating the MA interface with N inhibits the growth of oxides, maintaining high Q over time.

NbN-based superconducting qubits have reached a relaxation time of 16 μs.[28] However, the performance of these devices is still below the state of the art, necessitating further investigation of NbN films. If a resonator could have the MA interface from a nitride superconductor and the MS interface from an elemental superconductor, then its microwave loss caused by TLS is expected to be extremely low. There have been attempts to deposit a thin TiN film covering Nb to prevent the growth of NbO_x,[29] but the sidewalls are not covered by TiN and can still oxidize.

Nitrogen doping[30] is a well-established technique used to create low-loss Nb 3D cavities. By baking the Nb cavity in N_2 gas at a temperature above 800 °C, a conformal layer of NbN_x is formed at the MA interface, which inhibits the growth of surface oxide.[31] In theory, this method can be adapted to make planar superconducting devices; however, the effect of high temperature is not yet well understood. Treatment at high temperature can change the stress and grain size of the deposited metal and allow Nb to diffuse into the Si substrate, which all could potentially affect microwave loss.[32–34] Baking at high temperature can also introduce dislocation and vacancy defects in the Si substrate, whose effects on microwave loss have not yet been systematically explored.

In this Letter, we demonstrate nitrogen doping of Nb CPW resonators without introducing potentially performance-limiting defects related to high temperature. We utilize a radio frequency (RF) plasma to satisfy the activation energy required for nitrogen doping. We show that a N_2 plasma at 300 °C for 10 min dopes the top 5 nm of the Nb surface with N, which suppresses the growth of Nb oxides at the surface. Furthermore, we demonstrate that the passivation remains robust in an ambient air environment for sufficiently long periods of time to incorporate passivated Nb structures into complex, multi-layer quantum processors. Our process can be easily manifested with equipment available in typical industrial and academic facilities.

The films used in this study are fabricated by first cleaning a 2-in. intrinsic Si (111) wafer[35] with resistivity greater than 8000 Ω·cm in piranha solution (3:1 mixture of H_2SO_4 and H_2O_2) at 120 °C for 10 min followed by a BOE clean (7:1 mixture of NH_4F and HF) for 5 min. We then load the wafer into an electron-beam evaporation chamber (AJA ATC-ORION-8E) in less than 3 min. We evaporate 250 nm of Nb (99.95% purity) at a chamber pressure of $3 \cdot 10^{-9}$ Torr and a rate of 2 nm/min[36,37] at room temperature, resulting in a thickness uniformity better than 2.5% variation. The thickness of the Nb film is confirmed by crystal microbalance and profilometer measurements.

The resonator pattern is defined after we deposit the Nb film and before the passivation steps. We utilize a positive photoresist (MicroChem Shipley S1805) and a 375 nm optical direct-write laser lithography system (Heidelberg DWL 66+) to pattern the film. We etch the patterned film using a mixture of SF_6 and Ar in an reactive ion etch (RIE) system (Oxford Plasma Lab 100 ICP). Our etching recipe produces a 550 ± 20 nm deep trench in the Si substrate. We then oxygen plasma ash the samples (100 W, 15 sccm O_2) for 30 s and finally soak them in MicroChem Remover PG for >8 h at 70 °C to remove the remaining resist.

To passivate the samples, we start by performing a BOE clean for 30 min to remove all the surface oxide before transferring the wafer into a plasma-enhanced chemical vapor deposition (PECVD) chamber (Oxford Instruments Nanofab). The transfer time between removal from the BOE solution and evacuation of the PECVD chamber is kept below 3 min. We first let the wafer sit at 300 °C for 10 min with 1200 sccm N_2 flow and a chamber pressure of 1 Torr. We then start a 20 W RF plasma at the same chamber condition for 10 min. Finally, we cool down the chamber to 100 °C with 100 sccm of N_2 flow over the course of one hour before removing the sample. The passivation process forms a ∼2 nm thick SiN_x layer at the exposed Si surface in the trench area. We perform a third BOE clean for 15 s to remove this thin SiN_x layer.

The PECVD system uses a routine process to remove oxides from the chamber walls. This process introduces residual F in the chamber, which reacts with the Nb films. To mitigate contamination from F, we deposit ∼1 μm of SiO_x on a dummy wafer and the chamber wall immediately before passivating our sample.

We characterize the surface atomic species of passivated and unpassivated Nb films using X-ray Photoelectron Spectroscopy (XPS). The XPS system (Physical Electronics 5000 VersaProbe II Scanning ESCA Microprobe) uses an Al K_α line source and *in situ* Ar ion milling to facilitate analysis of material at depth. Figure 2(a) shows the XPS scan of a passivated Nb film with its top 1 nm removed. The observed peak corresponds to N 1s electrons. We fit the N 1s peak to a pseudo-Voigt function and the background to a linear function. We use the same practice to fit all the N 1s and O 1s[38] peaks measured in this study.

Figure 2(b) shows the area under the N 1s peak as a function of surface material removed for Nb films with different treatments. The untreated sample and the sample that is simply annealed in N_2 at 300 °C without lighting a plasma do not show a strong N presence. In comparison, a plasma passivated Nb film shows a well-defined N peak

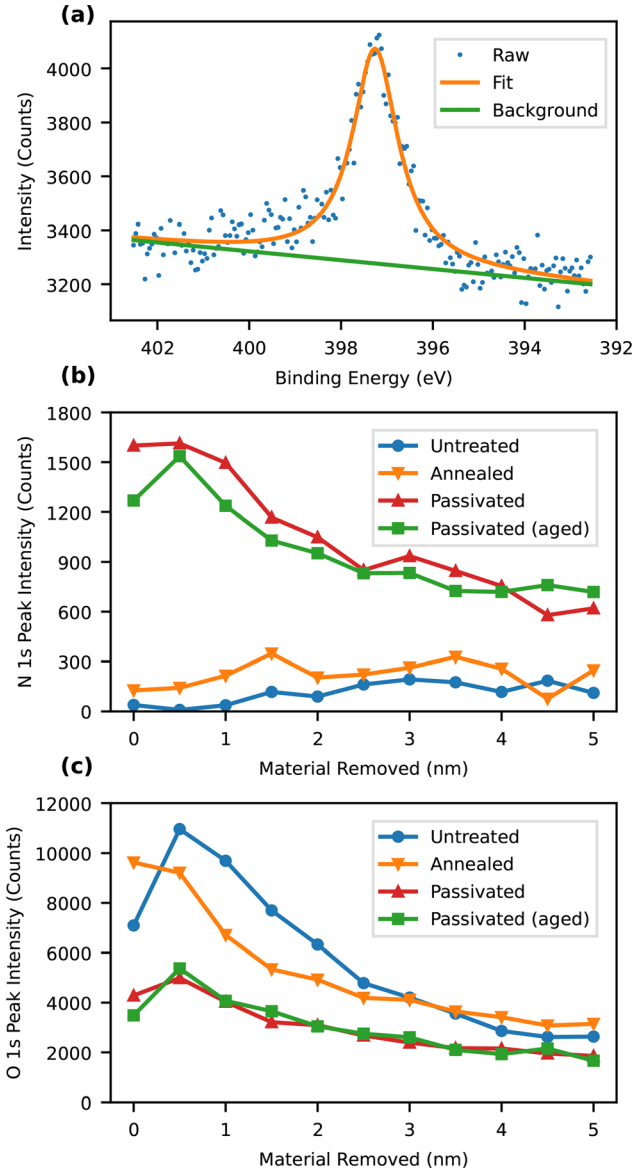

FIG. 2. Effect of different surface treatments on the XPS 1s peak of N and O. (a) The observed N 1s peak for a passivated Nb film at 1 nm depth. (b) and (c) The N 1s peak (b) and the O 1s peak (c) for different film treatments as a function of etch depth by *in situ* Ar ion milling.

that persists to a depth of 5 nm, which suggests successful incorporation of N atoms. The intensity of the N peak does not change significantly after we age the passivated Nb sample in an ambient environment for 15 days. In Fig. 2(c), we show that the presence of O in the top 5 nm of the surface is reduced for passivated samples. Similar to N, the O concentration in the plasma passivated sample does not change after being aged in an ambient environment for 15 days.

The study of N and O 1s electrons confirms a suppressed oxygen concentration near the surface for passivated samples. We now examine the Nb 3d electrons to investigate the oxides present near the surface of the films. Figure 3 shows the raw XPS spectrum of the different chemical states of the Nb 3d peaks from the same samples shown in Fig. 2. As the stoichiometry of the oxide layer is complex[39] and we have also introduced a nitride with unknown stoichiometry, we expect the spectrum to contain at least 10 individual peaks that overlap with each other. We examine the trend of the energy shift of the dominant peaks from an oxygen-rich high binding energy to lower binding energies, which are associated with states that are less oxygen-rich. At zero depth [Fig. 3(a)], we observe clear Nb 3d doublet peaks corresponding to Nb_2O_5 at 207.5 and 210 eV for the unpassivated sample. These two peaks shift to lower energies of 206.8 and 209.3 eV for the passivated films, which correspond to a less oxygen-rich Nb oxide state. The un-oxidized Nb 3d doublet peaks are also clearly present at 201.8 and 204.3 eV for the passivated sample. As shown in Fig. 3(b), the unpassivated sample has two dominant peaks at ~203.5 and ~206.5 eV and a small peak at 210 eV. We associate this with a combination of NbO, Nb_2O_5, and a large population of NbO_2. In comparison, the dominant peaks of the passivated sample are at 202.6 and 205.3 eV, which we attribute to a majority of NbO and NbN together with a small amount of Nb. We also observe that the Nb XPS spectrum does not change significantly for the passivated sample after 15 days of aging in an ambient environment. This indicates that the passivated sample does not accumulate significantly more oxide over this period of time.

To study the effect of the passivation process on the quality of the Nb films, we measure the direct-current (DC) resistance of the passivated and the untreated films as a function of temperature using a four-point technique inside a Quantum Design physical property measurement system (PPMS). Both samples are diced from the same Nb film deposited on the same Si (111) wafer allowing us to attribute the change in film properties to the passivation process alone. We extract the residual resistivity ratio (RRR) by taking the ratio between the resistance value at 297 and 10 K. We find that the untreated sample has a RRR of 4.86, which is similar to our previous result on Si (100).[37] The plasma passivated sample has a reduced RRR value of 2.96. Figure 4(a) shows the resistance near the superconducting transition of both samples. We observe a superconducting critical temperature T_c of 9.28 ± 0.05 K for the untreated sample and a suppressed T_c of 8.49 ± 0.05 K for the plasma passivated sample with T_c taken from the temperature value when the resistance drops to half of its residual value in the normal state. The suppressed T_c can be explained by assuming that the top NbN_x passivation layer is disordered and, therefore, has a much lower T_c than the Nb film. Given the bilayer system, we can estimate the thickness of NbN_x to be about 14.5 nm in agreement with our observation from the XPS data that N atoms extend at least 5 nm into the surface.[40,41] We further estimate the zero-temperature penetration depth to be 77 nm for the untreated film and 97 nm for the passivated film.[41–43]

Figure 4(b) shows the x-ray diffraction (XRD) spectrum of both samples measured in a Rigaku MiniFlex system with a Cu K_α source. Although both samples show similar texture, the Nb (110) peak of the passivated sample has about half of the intensity compared to the untreated film. We do not observe any peaks that are associated with NbN_x, which confirms our assumption that the NbN_x layer is disordered.

We utilize cryogenic microwave measurements to extract the power-dependent quality factor of CPW resonator structures and to

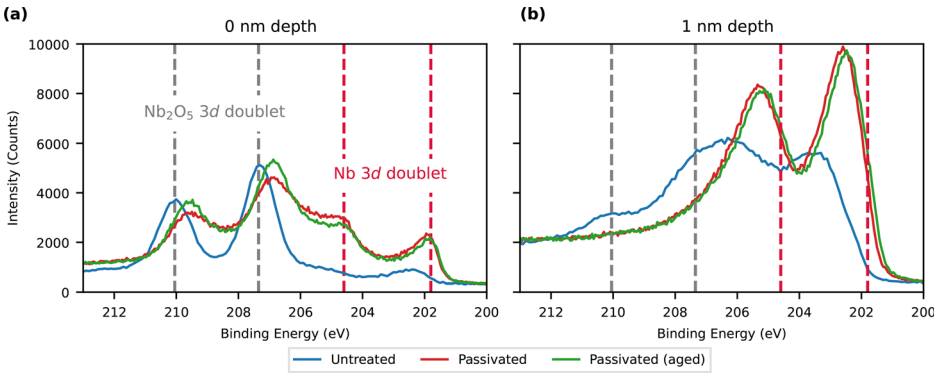

FIG. 3. XPS spectrum of the Nb 3d peaks with (a) 0 nm and (b) 1 nm of the surface material removed.

study the effect of passivation on the TLS-induced loss in the devices. We apply the passivation process to the resonators after the CPW structures are defined with RIE so that the sidewalls of the resonators are also passivated. The resonators are capacitively coupled to a transmission line with coupling quality factor $Q_c \simeq 0.5 \times 10^6$. Hanger-style resonators[37,44] with two types of geometries are fabricated. The first geometry has a center strip width of 3 μm, gap width of 2 μm, and has a continuous ground plane. This design allows us to clearly observe the effect of TLSs by maximizing capacitive dielectric loss[13] and minimizing inductive[45,46] and radiative[47] losses. The second geometry has a center strip width of 20 μm and a gap width of 12 μm and has holes (5×5 μm^2 squares) periodically (every 15 μm) etched into the ground plane.[48] This design minimizes the capacitive loss but is more susceptible to radiative loss[47] and loss caused by trapped magnetic flux.[45] We use LakeShore VGE-7031 insulating varnish to attach each resonator sample to a microstrip-style microwave launch with Pd-coated Cu metallization and Rogers Duroid 6010LM dielectric. We make three wirebonds to each port with 1 mil Al-1% Si bonding wire. The microstrip launch is enclosed inside a Pd-coated Cu sample package. The package is cooled inside a Rainier Model 103 adiabatic demagnetization refrigerator (ADR) down to 50 mK. We add ~100 dB of attenuation distributed among different temperature stages to the input line.[44] We shield the sample from stray magnetic fields with a high permeability can (Amuneal Cryoperm) surrounding the sample package. The output of the sample passes through one circulator to a high-electron-mobility transistor (HEMT) amplifier at the 4 K stage. Further amplification is used at room temperature.

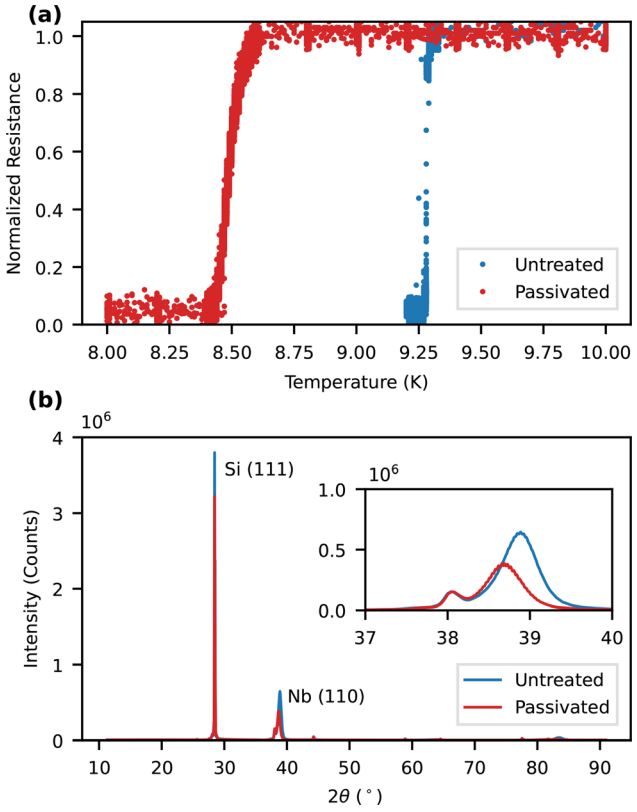

FIG. 4. (a) Superconducting transition of plasma passivated and untreated samples. (b) XRD 2θ scan of plasma passivated and untreated Nb films. The inset shows the Nb (110) peaks from Cu $K_{\alpha 1}$ and $K_{\alpha 2}$.

A vector network analyzer (VNA) is used to measure the transmission through the sample. The Q_i of each resonator is extracted at different average circulating photon numbers $\langle n \rangle$ ranging from ~1 to ~10^7 using the diameter correction method.[49] $F\delta_{TLS}$ and the high-power internal quality factor Q_i^{HP} are calculated from[8]

$$F\delta_{TLS}\frac{\tanh\left(\frac{hf}{k_BT}\right)}{\sqrt{1+\frac{\langle n\rangle}{n_c}}}=\frac{1}{Q_i^{HP}}-\frac{1}{Q_i}, \quad (1)$$

where h is the Planck constant, f is the resonant frequency of the resonator, k_B is the Boltzmann constant, T is the temperature of the resonator, and n_c is the critical photon number that differentiates the high and low power regions. When $\langle n \rangle$ is large, the contribution to microwave loss from saturable TLSs approaches zero, so Q_i^{HP} gives a good estimate of the other sources of loss, which mainly result from quasiparticles, trapped magnetic flux, and radiation.

Figure 5(a) shows a comparison of the $F\delta_{TLS}$ value among plasma passivated and untreated samples of both designs. Untreated resonators with the 3 μm center strip geometry have an average $F\delta_{TLS}$ of $(12.5 \pm 1.5) \cdot 10^{-7}$. This agrees with the result for untreated samples obtained in our previous study,[37] which uses the same design but

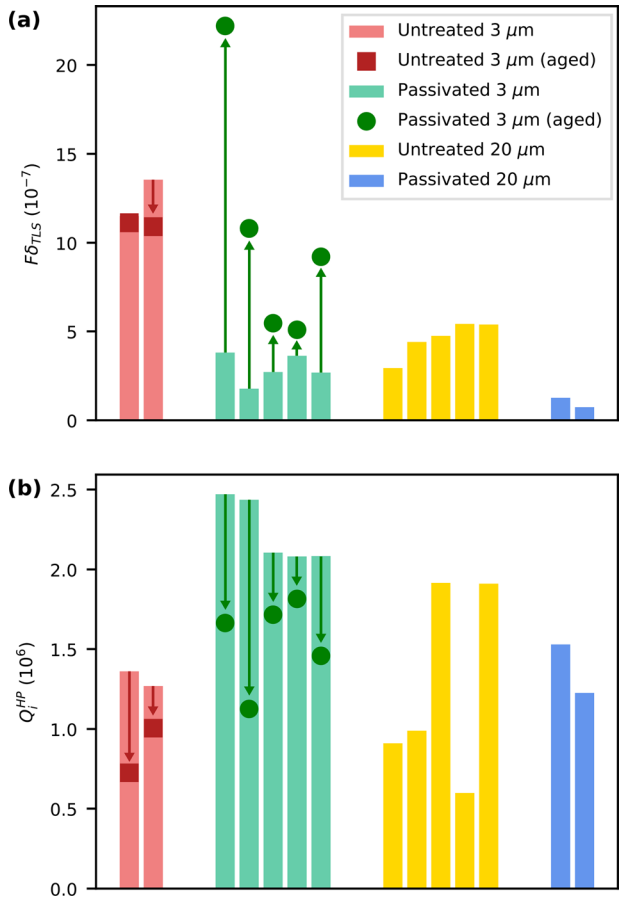

FIG. 5. Microwave performance of passivated and untreated samples. (a) Extracted $F\delta_{TLS}$ values among plasma passivated and untreated resonators with 3 and 20 μm center strip geometries. (b) Extracted Q_i^{HP} of the same resonators shown in (a).

intrinsic Si (100) wafers instead of Si (111). In comparison, the passivated resonators have an average $F\delta_{TLS}$ of $(2.9 \pm 0.5) \cdot 10^{-7}$, which is ~4 times lower than the untreated value. Resonators with the 20 μm center strip geometry have an average $F\delta_{TLS}$ of $(4.6 \pm 1.0) \cdot 10^{-7}$ for untreated samples and $F\delta_{TLS}$ of $(1.0 \pm 0.3) \cdot 10^{-7}$ for passivated samples. Figure 5(b) shows the extracted Q_i^{HP} of the same resonators shown in Fig. 5(a). Resonators with the 3 μm center strip geometry show an increased Q_i^{HP} compared to untreated devices. We attribute this potentially to a reduced TLS density in the regions of the sample that are too far from the resonators to be effectively saturated at high power and reduced spin defects residing in the Nb_2O_5 layer.[14] The Q_i^{HP} values of the resonators with the 20 μm center strip geometry are less uniform. We suspect that this could be due to their susceptibility to trapped vortices and radiation to lossy regions inside the package. The Q_i^{HP} values of our resonators are lower compared to other similar studies,[17,32] which we attribute to specific details of the sample package[47,50] and measurement setup.

To test the stability of the passivated samples over time, we allow some of the samples to age in an ambient environment for 45 days. Figure 5(a) indicates the change in $F\delta_{TLS}$ after this aging duration. We observe negligible change in $F\delta_{TLS}$ for the untreated devices, indicating that the oxide had already reached self-limited thickness before the first measurement. The passivated resonators exhibit increased $F\delta_{TLS}$ of varying degrees. In particular, two of the five passivated resonators maintained a significantly lower $F\delta_{TLS}$ compared to the untreated resonators, validating the stability of the passivated samples. Three of the passivated resonators, however, exhibited a significant increase in $F\delta_{TLS}$, which could be due to additional contamination of the resonators during storage. Visual inspection reveals significant residue and debris in the gap regions of CPWs for the resonators with significantly increased $F\delta_{TLS}$. We attribute this debris to the process of removing, storing, and re-gluing samples into the sample package for the second measurement. In Fig. 5(b), we indicate the change in Q_i^{HP} for the aged devices. For all samples, we observe a reduction in Q_i^{HP} after aging.

We extract the filling factor of the MA and MS interface based on a simulation of the cross section of the resonators with a 3 μm center strip using a HFSS Q3D extractor. By assuming a dielectric constant (thickness) of 41 (5 nm) for the MA interface and of 4 (2 nm) for the SA interface, we obtain a filling factor of $2.3 \cdot 10^{-5}$ for the MA interface and $5.0 \cdot 10^{-4}$ for the SA interface, both of which scale linearly with their thickness. By assuming a loss tangent of $9.9 \cdot 10^{-3}$ for Nb_2O_5 and $1.7 \cdot 10^{-3}$ for SiO_x,[12,16] we obtain a total loss of $1.08 \cdot 10^{-6}$, which agrees with our results of the untreated devices. The microwave loss of the passivated devices agrees with the loss estimated with a 1.3 nm thick Nb_2O_5 layer and a 0.5 nm thick SiO_x layer. As we do not observe a significant change in the O population from the XPS scan, we assume the increase in the microwave loss comes mainly from the increase in SiO_x thickness from 0.5 nm to 1 nm, which is expected from exposing Si to ambient conditions.[51]

Our study demonstrates a recipe for passivation of Nb structures with the nitrogen plasma, which dopes the top 5 nm of the Nb surface with N atoms. These N atoms suppress the O concentration and, therefore, reduce the amount of TLS defects that induce microwave loss. The N and O populations are stable after 15 days of aging in ambient air according to XPS measurements. Cryogenic microwave measurements confirm that our passivation process reduces the microwave loss of CPW resonators of two different design geometries. Our process removes the stringent time sensitivity associated with the regrowth of NbO_x and allows for the incorporation of low microwave loss Nb structures into state-of-the-art quantum processors. Our process also creates a platform on which other sources of microwave loss can be further studied. Although T_c and XRD measurements suggest that our process creates a more disordered superconductor, which may increase the susceptibility to losses caused by quasiparticle and magnetic vortices, these mechanisms do not yet dominate the microwave loss. While the side effect of suppressed superconductivity may be reduced by starting with Nb films with large grain size and longer electron mean free path, the suppressed superconductivity may also be useful in producing low loss kinetic-inductance-based sensors.[52,53] As Ta also has a superconducting nitride[54] and is more refractory than Nb, our passivation process may also work in reducing the microwave loss of Ta.

This research was supported by NSF Grant No. PHY-1752844 (CAREER), Air Force Office of Scientific Research (AFOSR) Multidisciplinary University Research Infinitive (MURI) Award on Programmable systems with non-Hermitian quantum dynamics (Award No. FA9550-21-1-0202), DOE Grant No. DE-SC0017987,

and the John Templeton Foundation, Grant No. 61835. The authors acknowledge the use of facilities at the Institute of Materials Science and Engineering in Washington University.

AUTHOR DECLARATIONS

Conflict of Interest

The authors declare no competing interests.

DATA AVAILABILITY

The data that support the findings of this study are available from the corresponding author upon reasonable request.

REFERENCES

[1]F. Arute, K. Arya, R. Babbush, D. Bacon, J. C. Bardin, R. Barends, R. Biswas, S. Boixo, F. G. S. L. Brandao, D. A. Buell, B. Burkett, Y. Chen, Z. Chen, B. Chiaro, R. Collins, W. Courtney, A. Dunsworth, E. Farhi, B. Foxen, A. Fowler, C. Gidney, M. Giustina, R. Graff, K. Guerin, S. Habegger, M. P. Harrigan, M. J. Hartmann, A. Ho, M. Hoffmann, T. Huang, T. S. Humble, S. V. Isakov, E. Jeffrey, Z. Jiang, D. Kafri, K. Kechedzhi, J. Kelly, P. V. Klimov, S. Knysh, A. Korotkov, F. Kostritsa, D. Landhuis, M. Lindmark, E. Lucero, D. Lyakh, S. Mandrà, J. R. McClean, M. McEwen, A. Megrant, X. Mi, K. Michielsen, M. Mohseni, J. Mutus, O. Naaman, M. Neeley, C. Neill, M. Y. Niu, E. Ostby, A. Petukhov, J. C. Platt, C. Quintana, E. G. Rieffel, P. Roushan, N. C. Rubin, D. Sank, K. J. Satzinger, V. Smelyanskiy, K. J. Sung, M. D. Trevithick, A. Vainsencher, B. Villalonga, T. White, Z. J. Yao, P. Yeh, A. Zalcman, H. Neven, and J. M. Martinis, "Quantum supremacy using a programmable superconducting processor," Nature **574**, 505–510 (2019).

[2]P. Jurcevic, A. Javadi-Abhari, L. S. Bishop, I. Lauer, D. F. Bogorin, M. Brink, L. Capelluto, O. Günlük, T. Itoko, N. Kanazawa, A. Kandala, G. A. Keefe, K. Krsulich, W. Landers, E. P. Lewandowski, D. T. McClure, G. Nannicini, A. Narasgond, H. M. Nayfeh, E. Pritchett, M. B. Rothwell, S. Srinivasan, N. Sundaresan, C. Wang, K. X. Wei, C. J. Wood, J.-B. Yau, E. J. Zhang, O. E. Dial, J. M. Chow, and J. M. Gambetta, "Demonstration of quantum volume 64 on a superconducting quantum computing system," Quantum Sci. Technol. **6**, 025020 (2021).

[3]W. D. Oliver and P. B. Welander, "Materials in superconducting quantum bits," MRS Bull. **38**, 816–825 (2013).

[4]C. E. Murray, "Material matters in superconducting qubits," arXiv:2106.05919 (2021).

[5]B. Josephson, "Possible new effects in superconductive tunnelling," Phys. Lett. **1**, 251–253 (1962).

[6]P. W. Anderson and J. M. Rowell, "Probable observation of the Josephson superconducting tunneling effect," Phys. Rev. Lett. **10**, 230–232 (1963).

[7]A. D. O'Connell, M. Ansmann, R. C. Bialczak, M. Hofheinz, N. Katz, E. Lucero, C. McKenney, M. Neeley, H. Wang, E. M. Weig, A. N. Cleland, and J. M. Martinis, "Microwave dielectric loss at single photon energies and millikelvin temperatures," Appl. Phys. Lett. **92**, 112903 (2008a).

[8]C. R. H. McRae, H. Wang, J. Gao, M. R. Vissers, T. Brecht, A. Dunsworth, D. P. Pappas, and J. Mutus, "Materials loss measurements using superconducting microwave resonators," Rev. Sci. Instrum. **91**, 091101 (2020).

[9]A. Nersisyan, S. Poletto, N. Alidoust, R. Manenti, R. Renzas, C.-V. Bui, K. Vu, T. Whyland, Y. Mohan, E. A. Sete, S. Stanwyck, A. Bestwick, and M. Reagor, "Manufacturing low dissipation superconducting quantum processors," in *2019 IEEE International Electron Devices Meeting (IEDM)* (IEEE, 2019), pp. 31.1.1–31.1.4.

[10]A. P. M. Place, L. V. H. Rodgers, P. Mundada, B. M. Smitham, M. Fitzpatrick, Z. Leng, A. Premkumar, J. Bryon, A. Vrajitoarea, S. Sussman, G. Cheng, T. Madhavan, H. K. Babla, X. H. Le, Y. Gang, B. Jäck, A. Gyenis, N. Yao, R. J. Cava, N. P. de Leon, and A. A. Houck, "New material platform for superconducting transmon qubits with coherence times exceeding 0.3 milliseconds," Nat. Commun. **12**, 1779 (2021).

[11]J. Wenner, R. Barends, R. C. Bialczak, Y. Chen, J. Kelly, E. Lucero, M. Mariantoni, A. Megrant, P. J. J. O'Malley, D. Sank, A. Vainsencher, H. Wang, T. C. White, Y. Yin, J. Zhao, A. N. Cleland, and J. M. Martinis, "Surface loss simulations of superconducting coplanar waveguide resonators," Appl. Phys. Lett. **99**, 113513 (2011).

[12]A. Melville, G. Calusine, W. Woods, K. Serniak, E. Golden, B. M. Niedzielski, D. K. Kim, A. Sevi, J. L. Yoder, E. A. Dauler, and W. D. Oliver, "Comparison of dielectric loss in titanium nitride and aluminum superconducting resonators," Appl. Phys. Lett. **117**, 124004 (2020).

[13]C. Müller, J. H. Cole, and J. Lisenfeld, "Towards understanding two-level-systems in amorphous solids: Insights from quantum circuits," Rep. Prog. Phys. **82**, 124501 (2019).

[14]E. Sheridan, T. F. Harrelson, E. Sivonxay, K. A. Persson, M. V. P. Altoé, I. Siddiqi, D. F. Ogletree, D. I. Santiago, and S. M. Griffin, "Microscopic theory of magnetic disorder-induced decoherence in superconducting Nb films," arXiv:2111.11684 (2021).

[15]T. Proslier, M. Kharitonov, M. Pellin, J. Zasadzinski, and Ciovati, "Evidence of surface paramagnetism in niobium and consequences for the superconducting cavity surface impedance," IEEE Trans. Appl. Supercond. **21**, 2619–2622 (2011).

[16]J. Verjauw, A. Potočnik, M. Mongillo, R. Acharya, F. Mohiyaddin, G. Simion, A. Pacco, T. Ivanov, D. Wan, A. Vanleenhove, L. Souriau, J. Jussot, A. Thiam, J. Swerts, X. Piao, S. Couet, M. Heyns, B. Govoreanu, and I. Radu, "Investigation of microwave loss induced by oxide regrowth in high-Q niobium resonators," Phys. Rev. Appl. **16**, 014018 (2021).

[17]M. V. P. Altoé, A. Banerjee, C. Berk, A. Hajr, A. Schwartzberg, C. Song, M. A. Ghadeer, S. Aloni, M. J. Elowson, J. M. Kreikebaum, E. K. Wong, S. Griffin, S. Rao, A. Weber-Bargioni, A. M. Minor, D. I. Santiago, S. Cabrini, I. Siddiqi, and D. F. Ogletree, "Localization and reduction of superconducting quantum coherent circuit losses," arXiv:2012.07604 (2020).

[18]N. Cabrera and N. F. Mott, "Theory of the oxidation of metals," Rep. Prog. Phys. **12**, 163–184 (1949).

[19]K. Sokhey, S. Rai, and G. Lodha, "Oxidation studies of niobium thin films at room temperature by x-ray reflectivity," Appl. Surf. Sci. **257**, 222–226 (2010).

[20]K. Williams, K. Gupta, and M. Wasilik, "Etch rates for micromachining processing-part II," J. Microelectromech. Syst. **12**, 761–778 (2003).

[21]L. Zhang, L. You, L. Ying, W. Peng, and Z. Wang, "Characterization of surface oxidation layers on ultrathin NbTiN films," Physica C **545**, 1–4 (2018).

[22]M. R. Vissers, J. Gao, D. S. Wisbey, D. A. Hite, C. C. Tsuei, A. D. Corcoles, M. Steffen, and D. P. Pappas, "Low loss superconducting titanium nitride coplanar waveguide resonators," Appl. Phys. Lett. **97**, 232509 (2010).

[23]S. S. P. Rao, C. Hobbs, S. Olson, N. Foroozani, H. Chong, H. Stamper, B. Martinick, D. Ashworth, B. Bunday, M. Malloy, E. Holland, J. Nalaskowski, P. Kearney, T. Ngai, I. Wells, M. Yakimov, S. Oktyabrsky, B. O'Brien, V. Kaushik, K. A. Dunn, K. Beckmann, S. Bennett, M. Rodgers, T. Murray, S. Novak, B. Baker-O'Neal, C. Borst, K. D. Osborn, and M. Liehr, "Materials and processes for superconducting qubits and superconducting electronic circuits on 300 mm wafers," ECS Trans. **85**, 151–161 (2018).

[24]A. Shearrow, G. Koolstra, S. J. Whiteley, N. Earnest, P. S. Barry, F. J. Heremans, D. D. Awschalom, E. Shirokoff, and D. I. Schuster, "Atomic layer deposition of titanium nitride for quantum circuits," Appl. Phys. Lett. **113**, 212601 (2018).

[25]D. R. W. Yost, M. E. Schwartz, J. Mallek, D. Rosenberg, C. Stull, J. L. Yoder, G. Calusine, M. Cook, R. Das, A. L. Day, E. B. Golden, D. K. Kim, A. Melville, B. M. Niedzielski, W. Woods, A. J. Kerman, and W. D. Oliver, "Solid-state qubits integrated with superconducting through-silicon vias," npj Quantum Inf. **6**, 59 (2020).

[26]F. W. Carter, T. Khaire, C. Chang, and V. Novosad, "Low-loss single-photon NbN microwave resonators on Si," Appl. Phys. Lett. **115**, 092602 (2019).

[27]C. Sheagren, P. Barry, E. Shirokoff, and Q. Y. Tang, "Atomic layer deposition niobium nitride films for high-Q resonators," J. Low Temp. Phys. **199**, 875–882 (2020).

[28]S. Kim, H. Terai, T. Yamashita, W. Qiu, T. Fuse, F. Yoshihara, S. Ashhab, K. Inomata, and K. Semba, "Enhanced coherence of all-nitride superconducting qubits epitaxially grown on silicon substrate," Commun. Mater. **2**, 98 (2021).

[29]C. Berk, A. Banerjee, A. HAJR, J. M. Kreikebaum, V. Altoe, D. Santiago, D. F. Ogletree, and I. Siddiqi, "Improvement in superconducting resonator quality factor through surface passivation," Bull. Am. Phys. Soc. **66**, 1 (2021).

[30]A. Grassellino, A. Romanenko, D. Sergatskov, O. Melnychuk, Y. Trenikhina, A. Crawford, A. Rowe, M. Wong, T. Khabiboulline, and F. Barkov, "Nitrogen and argon doping of niobium for superconducting radio frequency cavities: A pathway to highly efficient accelerating structures," Supercond. Sci. Technol. **26**, 102001 (2013).
[31]G. D. L. Semione, A. D. Pandey, S. Tober, J. Pfrommer, A. Poulain, J. Drnec, G. Schütz, T. F. Keller, H. Noei, V. Vonk, B. Foster, and A. Stierle, "Niobium near-surface composition during nitrogen infusion relevant for superconducting radio-frequency cavities," Phys. Rev. Accel. Beams **22**, 103102 (2019).
[32]A. Megrant, C. Neill, R. Barends, B. Chiaro, Y. Chen, L. Feigl, J. Kelly, E. Lucero, M. Mariantoni, P. J. J. O'Malley, D. Sank, A. Vainsencher, J. Wenner, T. C. White, Y. Yin, J. Zhao, C. J. Palmstrøm, J. M. Martinis, and A. N. Cleland, "Planar superconducting resonators with internal quality factors above one million," Appl. Phys. Lett. **100**, 113510 (2012).
[33]A. Premkumar, C. Weiland, S. Hwang, B. Jäck, A. P. M. Place, I. Waluyo, A. Hunt, V. Bisogni, J. Pelliciari, A. Barbour, M. S. Miller, P. Russo, F. Camino, K. Kisslinger, X. Tong, M. S. Hybertsen, A. A. Houck, and I. Jarrige, "Microscopic relaxation channels in materials for superconducting qubits," Commun. Mater. **2**, 72 (2021).
[34]C. Kopas, M. K. Murthy, C. Gregory, B. I. Mercado, D. R. Queen, B. Wagner, and N. Newman, "Characterization of the chemical and electrical properties of defects at the niobium-silicon interface," arXiv:2011.08359 (2020).
[35]Since Nb does not match to the lattice of Si (111) or Si (100), we expect similar results independent of wafer orientation.
[36]S. Morohashi, N. Takeda, S. Tsujimura, M. Kawanishi, K. Harada, S. Maekawa, N. Nakayama, and T. Noguchi, "Characteristics of superconducting Nb layer fabricated using high-vacuum electron beam evaporation," Jpn. J. Appl. Phys., Part 1 **40**, 576–579 (2001).
[37]D. Kowsari, K. Zheng, J. T. Monroe, N. J. Thobaben, X. Du, P. M. Harrington, E. A. Henriksen, D. S. Wisbey, and K. W. Murch, "Fabrication and surface treatment of electron-beam evaporated niobium for low-loss coplanar waveguide resonators," Appl. Phys. Lett. **119**, 132601 (2021).
[38]A. V. Razinkin, E. Shalaeva, and M. V. Kuznetsov, "Photoelectron spectroscopy and diffraction of NbO_x/Nb (110) surface," Phys. Met. Metallogr. **106**, 56–66 (2008).
[39]J. Halbritter, "On the oxidation and on the superconductivity of niobium," Appl. Phys. A **43**, 1–28 (1987).
[40]L. N. Cooper, "Superconductivity in the neighborhood of metallic contacts," Phys. Rev. Lett. **6**, 689–690 (1961).
[41]A. I. Gubin, K. S. Il'in, S. A. Vitusevich, M. Siegel, and N. Klein, "Dependence of magnetic penetration depth on the thickness of superconducting Nb thin films," Phys. Rev. B **72**, 064503 (2005).
[42]M. Tinkham, *Introduction to Superconductivity: Second Edition*, Dover Books on Physics (Dover Publications, 2004).
[43]T. Van Duzer and C. Turner, *Principles of Superconductive Devices and Circuits* (Prentice Hall, 1999).
[44]D. S. Wisbey, M. R. Vissers, J. Gao, J. S. Kline, M. O. Sandberg, M. P. Weides, M. M. Paquette, S. Karki, J. Brewster, D. Alameri, I. Kuljanishvili, A. N. Caruso, and D. P. Pappas, "Dielectric loss of boron-based dielectrics on niobium resonators," J. Low Temp. Phys. **195**, 474–486 (2019).
[45]C. Song, T. W. Heitmann, M. P. DeFeo, K. Yu, R. McDermott, M. Neeley, J. M. Martinis, and B. L. T. Plourde, "Microwave response of vortices in superconducting thin films of Re and Al," Phys. Rev. B **79**, 174512 (2009).
[46]P. J. de Visser, J. J. A. Baselmans, S. J. C. Yates, P. Diener, A. Endo, and T. M. Klapwijk, "Microwave-induced excess quasiparticles in superconducting resonators measured through correlated conductivity fluctuations," Appl. Phys. Lett. **100**, 162601 (2012).
[47]S. Huang, B. Lienhard, G. Calusine, A. Vepsäläinen, J. Braumüller, D. K. Kim, A. J. Melville, B. M. Niedzielski, J. L. Yoder, B. Kannan, T. P. Orlando, S. Gustavsson, and W. D. Oliver, "Microwave package design for superconducting quantum processors," PRX Quantum **2**, 020306 (2021).
[48]I. Nsanzineza and B. L. T. Plourde, "Trapping a single vortex and reducing quasiparticles in a superconducting resonator," Phys. Rev. Lett. **113**, 117002 (2014).
[49]M. S. Khalil, M. J. A. Stoutimore, F. C. Wellstood, and K. D. Osborn, "An analysis method for asymmetric resonator transmission applied to superconducting devices," J. Appl. Phys. **111**, 054510 (2012).
[50]R. A. Matula, "Electrical resistivity of copper, gold, palladium, and silver," J. Phys. Chem. Ref. Data **8**, 1147–1298 (1979).
[51]M. Morita, T. Ohmi, E. Hasegawa, M. Kawakami, and M. Ohwada, "Growth of native oxide on a silicon surface," J. Appl. Phys. **68**, 1272–1281 (1990).
[52]J. Zmuidzinas, "Superconducting microresonators: Physics and applications," Annu. Rev. Condens. Matter Phys. **3**, 169–214 (2012).
[53]M. R. Vissers, J. Gao, M. Sandberg, S. M. Duff, D. S. Wisbey, K. D. Irwin, and D. P. Pappas, "Proximity-coupled Ti/TiN multilayers for use in kinetic inductance detectors," Appl. Phys. Lett. **102**, 232603 (2013).
[54]N. P. Breznay, M. Tendulkar, L. Zhang, S.-C. Lee, and A. Kapitulnik, "Superconductor to weak-insulator transitions in disordered tantalum nitride films," Phys. Rev. B **96**, 134522 (2017).